Separated Flow Response to Rapid Flap Deflection

Albert Medina*

Air Force Research Laboratory, Wright-Patterson AFB, OH, 45433

Maziar S. Hemati†

University of Minnesota, Twin Cities, Minneapolis, MN 55455

The aerodynamic response of a massively separated flow to rapid ramps in flap deflection angle is presented. A NACA0006 airfoil spanning the test section of a water tunnel is oriented at a fixed incidence of $20°$ for Reynolds number $Re = 40$k. The airfoil is bisected about the mid-chord position resulting in a 50%-chord trailing-edge flap, and is equipped with a suite of motors to produce a range of flap deflection frequencies and amplitudes. The objective is to ascertain the susceptibility of a massively separated flow to mechanical actuation and the viability of rapid flap deflection as a control mechanism. Focus is given to a deflection amplitude of $2°$ to minimize geometric deviation from the airfoil's baseline planar configuration. The flap ramp-maneuver is completed in a fraction of a single convective time. The desired response to such motions is the evocation of transients conducive to enhanced lift generation. Two distinct transient responses are produced pending the direction of flap deflection. In a rapid ramp resulting in a net increase in airfoil camber the lift is increased instantaneously to modest values before relaxation to the steady lifting state of the final deflection angle. In effect, this mode expedites convergence to the steady state value of the final airfoil configuration. Reversing the ramp direction, resulting in a net increase in camber, provokes a response characterized by an initial reduction in lift prior to achieving desired lift gains, followed by relaxation to steady state. Both modes prove disruptive to the leading-edge shear layer and both are cause for roll-up of a leading-edge vortex. Through proper orthogonal decomposition, it is revealed that within the most energetic modes of the flow response exists a polarity dependence on ramp direction with potential implication on how to incite an instantaneous response in flow actuation.

I.   Introduction

THE deleterious effects of flow separation in aerodynamics have long inspired pursuits toward active flow control with ambitions of mitigating performance degradation or expanding operational envelopes. Design objectives include lift enhancement, drag reduction, delayed onset of stall, and separation recovery for greater control-surface authority. To this end, there stands a need to develop a deeper understanding of the underlying phenomena associated with baseline separated flows and the receptivity of such flows to actuation. Such fundamental knowledge is necessary to furnish full-scale control applications where, as Williams et al. [1] concludes, improved lift control in unsteady flows requires improved understanding and modeling of the flow response to actuation, modeling of the unsteady aerodynamics, and a controller capable of reacting to these effects. It is therefore essential to measure the dynamic response of separated flows to actuator input when seeking predictive capabilities for an effective active flow control system. At the rudimentary level, quantifying the flow response to actuation is complicated by the unsteady nature of flow separation which bears host to a number of instabilities. As Raju et al. [2] identified, these instabilities can be categorized as Kelvin-Helmholtz instability within the leading-edge shear layer, shedding instability of the leading-edge vortex, and instability in the wake of the airfoil. The desired effect of actuation is then the suppression of instabilities near their respective sites of inception to mitigate propagation and amplification into the global flow field.

---

*Research Scientist, Spectral Energies, Aerodynamic Technology Branch, Aerospace Vehicles Division, Aerospace Systems Directorate, AIAA Senior Member.

†Assistant Professor, Department of Aerospace Engineering and Mechanics, AIAA Senior Member.

American Institute of Aeronautics and Astronautics

The fundamental lift response resulting from impulse-like actuator input has been a ubiquitous initial lift reversal followed shortly by a surge in lift incremented above the steady baseline performance before relaxation to an undisturbed state. Under single pulse actuation by Lorentz force Albrecht et al. [3] demonstrated insensitivity in the resultant lift transient profile to the actuation direction, be it oriented downstream or upstream. Although actuator direction proved influential on the initial development of the shear layer and the initiation of the reattachment process, the separation envelope bore the same response irrespective of pulse direction. Experiments by Brzozowski et al. [4] examined the receptivity of the separated flow above a stalled airfoil to a single short pulse ($t_{\text{pulse}}U/c = 0.04$) employing pulse-combustion actuators. Brzozowski et al. describes two prominent effects observed within the separated flow dynamics in response to actuation: (1) the severance of the separated vorticity layer from the airfoil surface and (2) ensuing advection of a large-scale clock-wise vortex, and secondly the roll-up of a co-rotating vorticity layer that advects along the airfoil surface. A momentary decrease in circulation was said to be attributed to the shedding of the severed clock-wise vortex, and the formation and advection of the surface shear layer led to a net increase in circulation and lift. Through continuous actuation, several works have demonstrated the ability to sustain flow reattachment to the airfoil. However, as Amitay and Glezer determined [5, 6], the transient response to step-change or pulse-like actuator input could be utilized in transient actuator pulses to generate higher lift coefficients than could be obtained through continuous actuation. Similarly, Margalit et al. [7] found a short duty cycle to be of substantial influence on the normal force coefficient corresponding to a delta wing platform at high incidence angle.

The aforementioned works are in concordance in their spatial selection of actuation favoring proximity to the leading edge. The anterior placement is localized near the separated shear layer in a targeted effort at favorably disrupting the baseline flow. The emphasis on placement is further reinforced in recognition of its crucial role in governing the effectiveness of a given actuator. Methods proposed by Natarajan et al. [8] and Chomaz [9] have provided frameworks to inform the placement of actuation sites by identification of spatial locations of maximum receptivity in the system. The effective locations of control are obtained by the overlap of forward and adjoint global modes of the system corresponding to regions of high dynamic sensitivity. However, with an objective of generating enhanced lift, the proper placement of an actuator may prove actuator-specific. In instances of employing blowing control, simulations by Huang et al. [10] highlighted the dependency of elevated lift on chord-wise location where greater lift was produced with actuation applied further downstream of the airfoil leading edge, peaking at $0.8c$ for tangential blowing. The resulting mechanism by which lift was enhanced did not appear contingent on excitation of the leading-edge flow field.

In the present study a NACA0006 airfoil is held at fixed incidence of $20°$ presenting a prototypical massively separated state. The susceptibility of the deep-stalled airfoil to discrete low-amplitude rapid flap motions is investigated. This work is distinguished from literature in its application of posterior mechanical actuation to incite leading-edge transient phenomena conducive to lift enhancement. In the current measurements, a case is made for the receptivity of a massively separated flow to rapid-ramp flap-maneuvers through examination of the lift response to ramp-rate and through interrogation of the resultant flow field's temporal evolution. Results highlight a means of flap actuation capable of generating favorable lift transients devoid of the classical 'lift reversal' but instead an instantaneous incremented lift.

II. Experimental Setup

Experiments were performed in the U.S. Air Force Research Laboratory (AFRL) Horizontal Free-Surface Water Tunnel (Fig. 1, *left*). The tunnel has a 4:1 contraction and 46-cm-wide by 61-cm-high test section with a free-surface speed range of 3-105cm/s and a streamwise-component turbulence intensity of $\sim 0.4\%$ at 15-40cm/s. The tunnel is fitted with a three-degree-of-freedom motion stage, consisting of a triplet of H2W Technologies linear motors, driven by AMC DigiFlex servo drives interfaced with a Galil DMC 4040 four-axes motion controller with user-selected proportional-integral-derivative gain constants for each axis. A plastic 3-D printed NACA 0006 airfoil of 200mm chord (physical aspect ratio of 2.25), strengthened by spanwise carbon-fiber rods, is bisected about the mid-chord position (Fig. 1, *right*). The test article spans the test section with a nominal 1mm gap at each wingtip. The resulting fore element is rigidly connected to the plunge rod of the front vertical linear motor. The resulting aft element, or flap, is analogously connected to the rear vertical linear motor, but is constrained by a linkage mechanism to the fore element such that relative motion between the two vertical motors results in a pitching motion of the flap. The fore element is

American Institute of Aeronautics and Astronautics

held at fixed incidence (which can be changed by swapping out its mounting arm), whereas the rear element is so displaced that its motion relative to the fore element enacts a pivot about the gap between the two airfoil elements. This gap measures 0.5 mm and is bridged with a flexible rubber film of 0.2mm thickness to prevent flare-up. Flap incidence angle is limited to $\pm 45°$ with respect to the horizontal plane. The fore element fixed-incidence angle is $\alpha_{\text{LE}} = 20°$, corresponding to a prototypical separated flow [11].
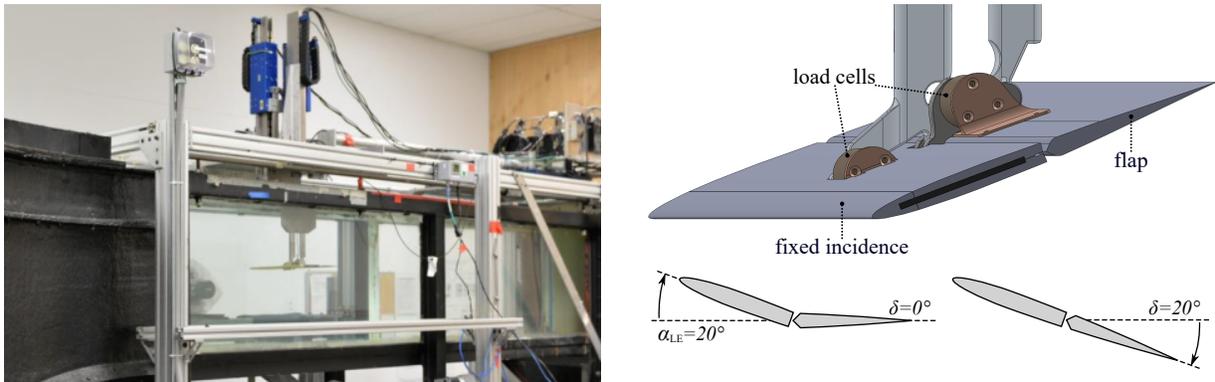

Figure 1. (*left*) **Water tunnel facility.** (*right*) **NACA0006 configuration and angular definitions.**

Force measurement was conducted via two ATI NANO-25 IP68 six-component force balances. Each airfoil element was supplied a dedicated force balance affixed to its respective frame. Importantly, there is no mechanical connection between the fore and aft elements; the forces of each element were therefore measured independently. Measurements were sampled at a rate of 1kHz and treated with a Butterworth low-pass filter of 8Hz. Force histories were constructed from ensemble averaging over ten consecutive runs. Static forces were derived from time-averaging over a hold period of 10s for each flap deflection angle. Lift coefficient and pitching moment coefficient are non-dimensionalized as $C_L = \left(L/0.5\rho U^2 S \right)$ and $C_M = \left(M/0.5\rho U^2 Sc \right)$, where L is the measured lift, M is the pitching moment about the airfoil quarter-chord position, ρ is the fluid density, U is the free-stream velocity, S is the planform area, and c is the chord length.

Planar flow visualization was performed at the three-quarter span-wise position. Rhodamine-590 was introduced at the leading edge and the trailing edge of the airfoil and fluoresced by illumination of a Nd:YLF laser sheet (Photonics Industries DM50-527, 55mJ/pulse, 10kHz max). To minimize surface reflections the camera was outfitted with an optical filter (Tiffen, Orange 21) compatible with the fluorescence emission. Velocity field data was obtained by utilizing the same laser sheet setup to perform particle image velocimetry. The time-resolved PIV data is two-dimensional and two-component, confined to the in-plane velocity field. For seeding, Polyamide particles of 20μm-diameter (LaVision, SG=1.03) were introduced into the tunnel. Within the light sheet the x- and y-components of velocity are calculated by correlation of single-exposure, double-frame image pairs using Fluere (Ver. 1.3). Image pairs were correlated using multi-pass, multi-grid interrogation with window sizes 64×64 to 48×48 with 50% overlap to produce a mean signal-to-noise ratio of 5.4. Velocity fields presented in this work are the results of ensemble-averaging over five consecutive experimental runs.

The flap motion is described by four parameters: initial flap angle δ_0, final flap angle δ_F, frequency of motion f, and smoothing coefficient a. The kinematic schedule begins with a sinusoidal waveform, $\delta(t) = \delta_{\text{M}} + \delta_{\text{A}} \cos(2\pi f t)$, where δ_{M} is the mean incidence angle ($\frac{\delta_F + \delta_0}{2}$), δ_{A} is the deflection amplitude ($\frac{\delta_0 - \delta_F}{2}$), and f is the frequency in hertz. Then a C^∞-smoothing ramp function suggested by Eldredge et al. [12] is fitted to the sinusoidal waveform over a semi-period, resulting in a motion given by Eq. (1):

$$\delta(t) = \frac{k}{a}\ln\left[\frac{\cosh\left(a\left(t - t_1\right)U/b\right)}{\cosh\left(a\left(t - t_2\right)U/b\right)}\right] + \frac{\delta_{\text{F}} + \delta_0}{2} \tag{1}$$

where $k = \dot{\delta}_{\text{max}} b/2U$ is the nominal deflection rate, $a = \pi^2 k/\left(2|\delta_F - \delta_0|(1 - \sigma)\right)$ is the smoothing parameter, σ is a fitting parameter proposed by Granlund et al. [13], b is the semi-chord, and time constants t_1 and t_2 respectively correspond to the start and completion of flap motion for the unsmoothed deflection profile. The duration of the unsmoothed motion ($t_2 - t_1$) is derived by matching its ramp rate to the peak slope of the

American Institute of Aeronautics and Astronautics

sinusoidal waveform. The resulting smoothed motion preserves the sine-wave peak velocity. Flap incidence angles are measured with respect to the horizontal plane, as illustrated in Fig. 1 (*right*).

The free-stream speed is $U = 200$mm/s, which, with a 200mm chord, gives a nominal chord-based Reynolds number of $Re \sim 40$k in water maintained at room temperature ($\sim 20°$C). Conveniently, one convective time is also numerically 1s of wall-clock time. Thus, for a frequency of 1Hz the flap motion completes approximately over a semi-period of 0.5s, or one half of one convective time: $0.5tU/c$. The C^∞ smoothing slightly broadens the kinematic profile; a representative case is given in Fig. 2 (*left*). The effect of smoothing over a range of frequencies is presented with more rigor in Fig. 2 (*right*) where the original sinusoidal profile commences at $tU/c = 0$. The parametric space of interest is summarized in Table 1. Flow visualization was performed by injection of Rhodamine-590 dye at the 3/4 span-wise position of the fore-element leading edge and the flap-element trailing edge. The dye is fluoresced within a ~ 1mm-thick light sheet generated by a Nd:YLF laser, firing at 50Hz.

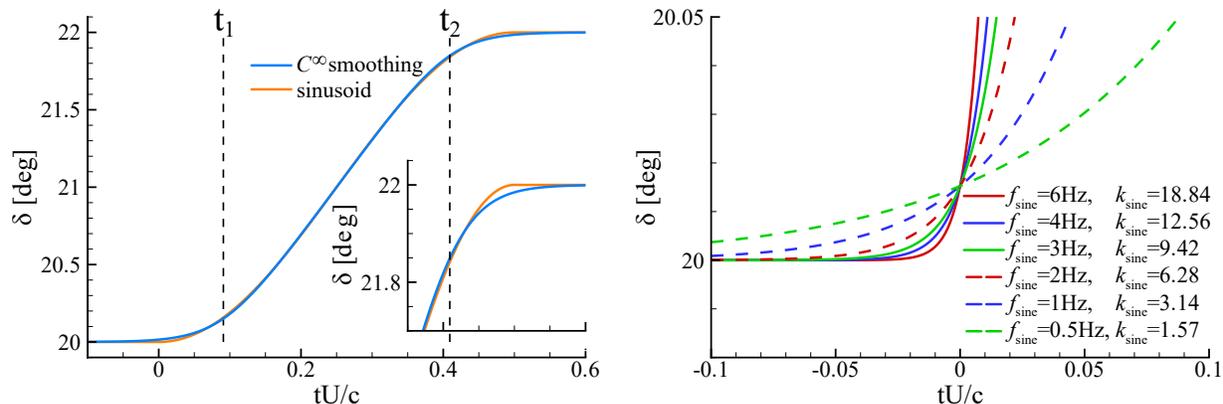**Figure 2. Typical kinematic profile for flap deflection: (*left*) C^∞-smoothing of a sinusoidal waveform, (*right*) effects of smoothing on kinematic start time.**

Table 1. Motion Parameters

$|\Delta\delta|$	f_{sine} [Hz]	k_{sine}	$|\dot\delta|_{\max}c/U$ [deg]
	0.5	1.5708	3.1416
	1	3.1416	6.2832
$2°$	2	6.2832	12.5664
	4	12.5664	25.1327
	6	18.8496	37.6991
	0.5	1.5708	1.5708
	1	3.1416	3.1416
$1°$	2	6.2832	6.2832
	4	12.5664	12.5664
	6	18.8496	18.8496

III. Results and Discussion

Direct force measurements and dye visualization were used to gauge the receptivity of a massively separated flow to rapid flap deflection. Here the term 'rapid' is reserved for flap deployments realized within one convective time. Employing a generously scaled flap as choice of control method is distinct from conventional mechanisms (be they jets, plasma, blowing/suction, acoustic forcing, or Lorentz forces) in that the flap is coupled with the airfoil geometry and the resulting aerodynamic signature. Any motions performed by the flap ultimately modify the lift capabilities of the airfoil by virtue of inciting transients in addition to reconfiguration of the lifting surface. Nevertheless, flap actuation still abides by many of the parameters

of its more modern counterparts: excitation amplitude (deflection amplitude), excitation width (duration of deflection or deflection rate), and direction (net increase or decrease in camber). The greatest constraint of the proposed control method is the mechanical limitations of deflection amplitude (and perhaps the deflection rates required of excitation). Moreover, because the intention of rapid flap deflection is to reconcile the baseline separated state of the airfoil with a state of elevated lift performance, consideration is given to deflection amplitudes conducive to the nominal preservation of the planar airfoil configuration. Therefore focus is primarily given to a deflection step of $|\Delta\delta| = 2°$ $(= |\delta_F - \delta_0|)$ which presents minimal deviation from the initially non-deflected configuration and amounts to a change in effective attack angle of $\Delta\alpha_{eff} = 1°$ (as observed in baseline attached flow measurements [14]). Prior to examining the transient aerodynamic response, the static effects of flap deflection on a baseline separated flow ($\alpha_{LE} = 20°$) are described.

A.   Baseline Performance: Static Survey

Results for static lift and drag coefficient in response to flap deflection are shown in Fig. 3(*left*). Total lift production exceeds drag for all deflection angles considered, $\delta = [0 - 40°]$. The resulting lift slope is roughly constant with total C_L bearing an approximate linear dependence on flap deflection. Total drag coefficient C_D appears to adhere to a polynomial trajectory, increasing with deflection angle. The modular construction of the test article also grants force measurements of the individual fore (separated LE) and aft (flap) elements. The individual lift coefficients demonstrate a non-linear deflection-angle dependency particularly for $\delta > 20°$, whereas trends further diverge from lift trajectories set at $\delta < 20°$. The drag coefficients of the two elements resume the profile observed in C_D. Drag on the fore element exceeds that of the flap for all deflection angles until $\delta = 40°$ where the two profiles are unified. In its most streamlined configuration the flap is oriented parallel to the freestream at $\delta = 0°$ where it is in essence shielded by the leading element and offers little impedance to the free-stream flow. This configuration translates to negligible lift and drag production by the flap. The accompanying qualitative imaging presented in Fig. 3(*right*) is suggestive of the juxtaposition of the organization of separated structures with respect to trends in the aerodynamic forces. All flow snapshots evince considerable separation, evidenced by the shear layer emanating from the leading edge and no discernible reattachment to the airfoil further downstream. The shear layer appears subject to a Kelvin-Helmholtz instability which transitions into regions of enhanced mixing that are convected downstream. The relative trajectory of the shear layer diverges from the leading edge further upward with increasing deflection angle. The influence of trailing-edge formations on inducing a downward momentum on the shear layer are diminished with net increases in camber. Accordingly, greater deflection amounts to an increase of the recirculating region aboard the suction surface of the airfoil where speeds are reduced below that of the free-stream.
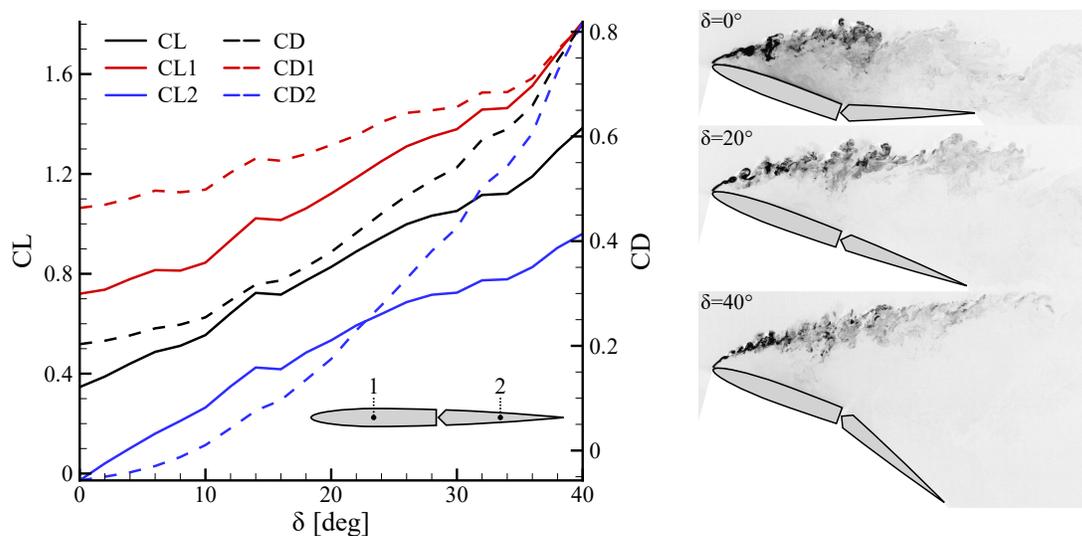

Figure 3.   Static lift and drag coefficient vs deflection angle $\delta = [0 - 40°]$: the leading element is at fixed incidence $\alpha_{LE} = 20°$. Deflection angle $\delta = 20°$ corresponds to a planar configuration.

B. Transient Response to Rapid Flap Deflection

The effect of a single low-amplitude ramp motion by the flap on the transient lift response of the separated airfoil was studied by direct force measurement. The leading element was held fixed at $20°$ incidence, and the flap concluded its motion at $\Delta\delta = \pm 2°$ from its initial angle of $\delta_0 = 20°$. As previously noted the deflection amplitude is intended to provide a minimal excursion from the initial planar airfoil configuration ($\alpha_{\mathrm{LE}} = \delta_0 = 20°$). The effects of a flap ramp-rate on lift and drag for $\Delta\delta = -2°$ (net decrease in positive camber) is shown in Fig. 4. Regardless of ramp rate, it should be understood that the lift and drag coefficients ultimately return to their respective asymptotic static values (Fig. 3) corresponding to the final flap angle. Barring the inertial or non-circulatory spikes associated with the acceleration phases of the flap, the ramp motion is cause for a transient spike in lift and drag exceeding static values. The dynamic lift profile that follows from the actuation period bears the hallmarks of the lift response observed in conventional control schemes [1]: immediately after actuation there exists a reduction in lift to a global minimum before steep surge culminating in a global maximum and then decreasing to a static value. The decremented state of lift persists for approximately $\Delta t U/c = 1.6$ (with respects to the initial deflection angle value) for ramp rates associated with $f \geq 2\mathrm{Hz}$. Within these speeds of operation the lift peak converges to $tU/c = 2.7$ with increasing ramp rate. The descent from peak lift is accentuated by a minor local peak nearing $tU/c = 5.4$ where lift production maintains a value in excess of the initial steady state.

Thus far the distinction has been made for rates associated with $f \geq 2\mathrm{Hz}$ where the characteristic response profile is readily identifiable, albeit scaled in some proportion to ramp rate. However, uniform among all the ramp rates of Fig. 4 is the initial decremented lift and the duration in which transients persist prior to recovery of a final steady state approaching $tU/c = 10$. The latter would suggest the duration of transient behavior scales as convective time rather than ramp rate. In this light, the ramp rate is suspected to incite a suite of flow dynamics above the airfoil, and the extent of their influence on the aerodynamic performance of the airfoil is predicated on the rate by which the flow structures are convected downstream. As the ramp rate is increased from $f = 1\mathrm{Hz}$ to $2\mathrm{Hz}$ the final lift response profile is quickly adopted. Furthermore, the scaling of the transient peak spike with increasing ramp rate may be indicative of lift saturation near $f = 6\mathrm{Hz}$.
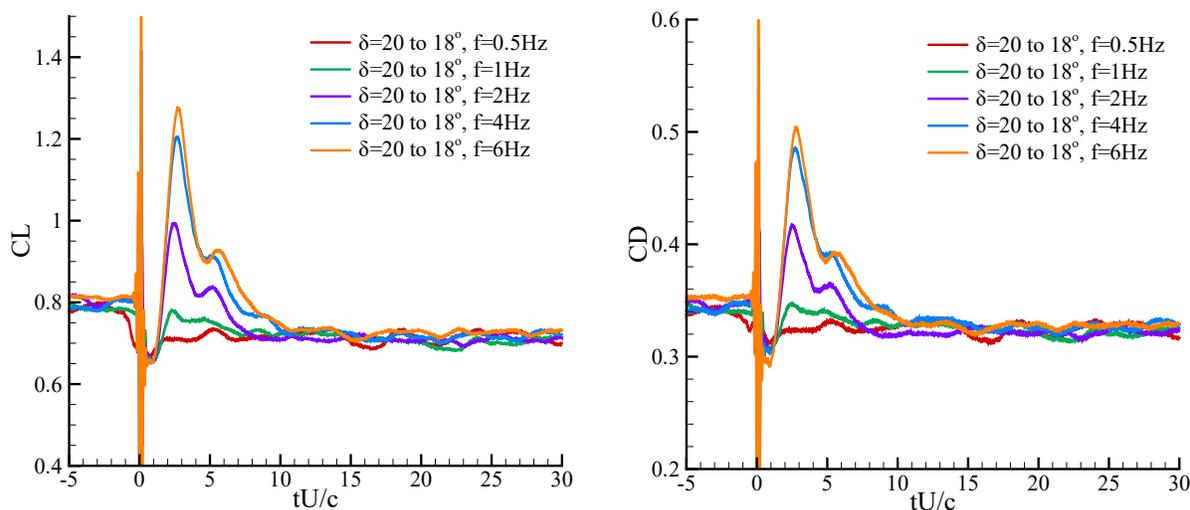

Figure 4. Lift and drag coefficient response to flap ramp-rate: $\delta = [20° - 18°]$, $f_{\mathrm{sine}} = [0.5, 1, 2, 4, 6]\,\mathrm{Hz}$. **Motion commences at** $tU/c = 0$.

Reversing now the ramp direction to $\Delta\delta = +2°$ (net increase in positive camber), the aerodynamic response to flap deflection from $\delta = 20°$ to $22°$ is made distinct from the $\Delta\delta = -2°$ case by its positive excitation time, transient profile, and lift increment. In contradistinction to the previous $\Delta\delta = -2°$ case, the airfoil experiences an immediate positive step in lift (and drag) coefficient in tandem with flap excitation, as shown in Fig. 5. The step in lift surpasses the steady state performance of $\delta = 22°$. This particular response mode is devoid of the deleterious negative lift spike characteristic of the conventional control mechanisms and demonstrates less variability among the transient responses corresponding to ramp rates of $f \leq 4\mathrm{Hz}$. The ensuing transient profile exhibits a primary and secondary peak before converging to a steady state

American Institute of Aeronautics and Astronautics

near $tU/c = 10$. In examination of Fig. 5, the disparity between peak lift production of deflection rate $f = 6$Hz and the remaining (lower) rates quickly becomes apparent with no immediately identifiable scaling guideline. This is to suggest the peak ramp rate examined here satisfies some circulatory threshold necessary to induce a transient profile reminiscent of a response previously reserved for $\Delta\delta = -2°$. The realization of an instantaneous response is in agreement with previous works exploring larger excursions from a planar configuration in baseline attached and separated states [15]. As previously alluded, the duration of the force transients appears independent of flap direction, be it $\Delta\delta = -2°$ or $+2°$. It is then apparent that the excitation of either of the two response modes is dependent on the direction of flap. Motions performed toward promoting net increase in positive camber incite the immediate incremental response and motions toward promoting a net decrease in positive camber generate a decremented lift state prior to realizing desired gains in lift. Lift measurements are repeated for $\Delta\delta = \pm1°$ in Fig. 6 which effective reduces the max ramp rate of $\Delta\delta = \pm2°$ by half. The two response modes are preserved along with their directional-deflection dependency.
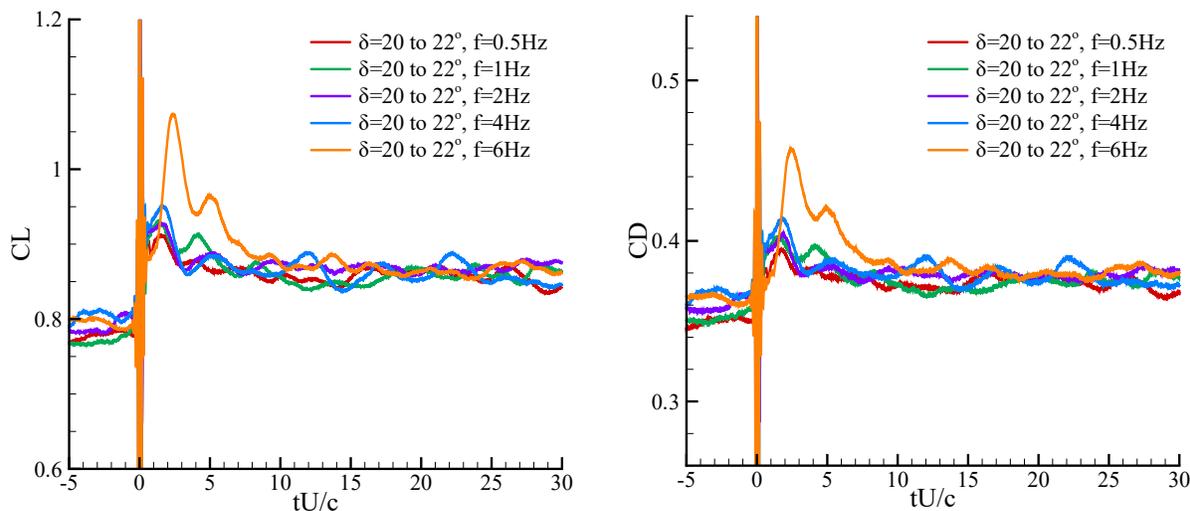

Figure 5. Lift and drag coefficient response to flap ramp-rate: $\delta = [20° - 22°]$, $f_{\text{sine}} = [0.5, 1, 2, 4, 6]$ Hz. **Motion commences at** $tU/c = 0$.
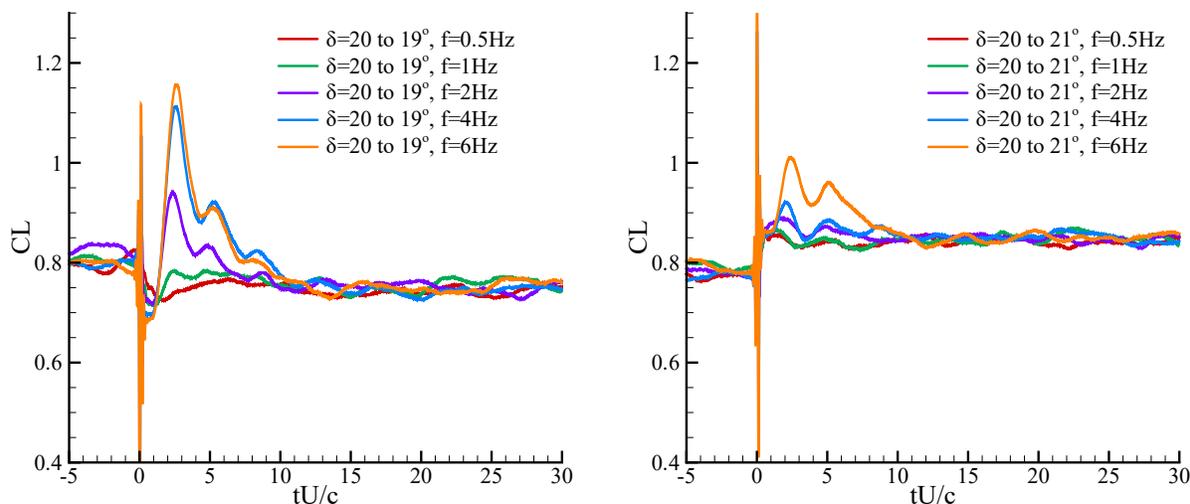

Figure 6. Lift coefficient response to flap ramp-rate: (*left*) $\delta = [20° - 19°]$, (*right*) $\delta = [20° - 21°]$, $f_{\text{sine}} = [0.5, 1, 2, 4, 6]$ Hz. **Motion commences at** $tU/c = 0$.

American Institute of Aeronautics and Astronautics

C. Flow Field Evolution for Rapid Flap Deflection

The flow visualizations of Fig. 7 document the accompanying temporal evolution of separated structures in response to a net-decreasing-positive-camber ramp ($\Delta\delta = -2°$) of $f = 6$Hz from an initial non-deflected configuration. Prior to flap motion at $tU/c = -0.5$ the flow field is characterized by the pronounced shear layer billowing from the leading edge of the airfoil, as noted in the static survey. Shortly after motion completes, the leading-edge shear layer is disrupted by the incipient roll-up of a discrete leading-edge vortex at $tU/c = 0.5$ corresponding to minimum lift generation. Concurrently, there exists shear roll-up about the airfoil trailing edge of comparable size to the leading-edge formation. The trailing-edge vortex is given rise by the termination of flap motion and by virtue of the new orientation. Further downstream the starting vortex associated with the initiation of flap motion is also visible in the near-wake. By $tU/c = 1.0$ lift still remains near the minimum value and both the leading-edge and trailing-edge vortices have grown about their respective edges to maintain comparable sizes. Their joint formation is cause for vertical expansion, or rather ejection, of the separated region as the previously disrupted shear layer formations navigate about the trailing-edge vortex periphery. The proximity of the trailing-edge vortex promotes a dominant clockwise swirl of the separated region. At this time the leading-edge vortex has appreciated in strength and begins to impose reattachment near the $0.3c$ chord position. Further reattachment is realized at $tU/c = 1.57$ where the bulk of the separated region has convected to the trailing edge, forming a counter-rotating vortex pair with the existing trailing-edge vortex. The reattachment point has shifted further along the chord to approximately $0.5c$ and the resulting lift resumes the initial steady state value of $\delta = 20°$. As the leading-edge continues to grow in size and strength at $tU/c = 2.0$, so too does the lift coefficient. The contour of the vortex adopts an elongated formation oriented nominally parallel to the airfoil surface. Peak lift production is achieved approaching $tU/c = 2.75$ where reattachment now approaches the trailing edge. The leading-edge vortex appears as an arch with the resumption of a sporadic leading-edge shear layer. The descent in lift is coincident with the bulk of the initial leading-edge roll-up traversing the chord and arriving at the trailing edge, as exemplified by $tU/c = 3.50$. The velocity induced at the trailing edge invites a layer of flow reversal that further removes the leading-edge vortex from the airfoil surface. The flow field is returned to its nominal initial steady state by $tU/c = 5.5$ with the exception of a streamlined near-wake. The effect is observed as the secondary local lift peak.

$\delta_0{=}20°$, $\delta_F{=}18°$

$\Delta tU/c{=}{-}0.50$ $\qquad$ $\Delta tU/c{=}0.50$ $\qquad$ $\Delta tU/c{=}1.0$

$\Delta tU/c{=}1.57$ $\qquad$ $\Delta tU/c{=}2.0$ $\qquad$ $\Delta tU/c{=}2.75$

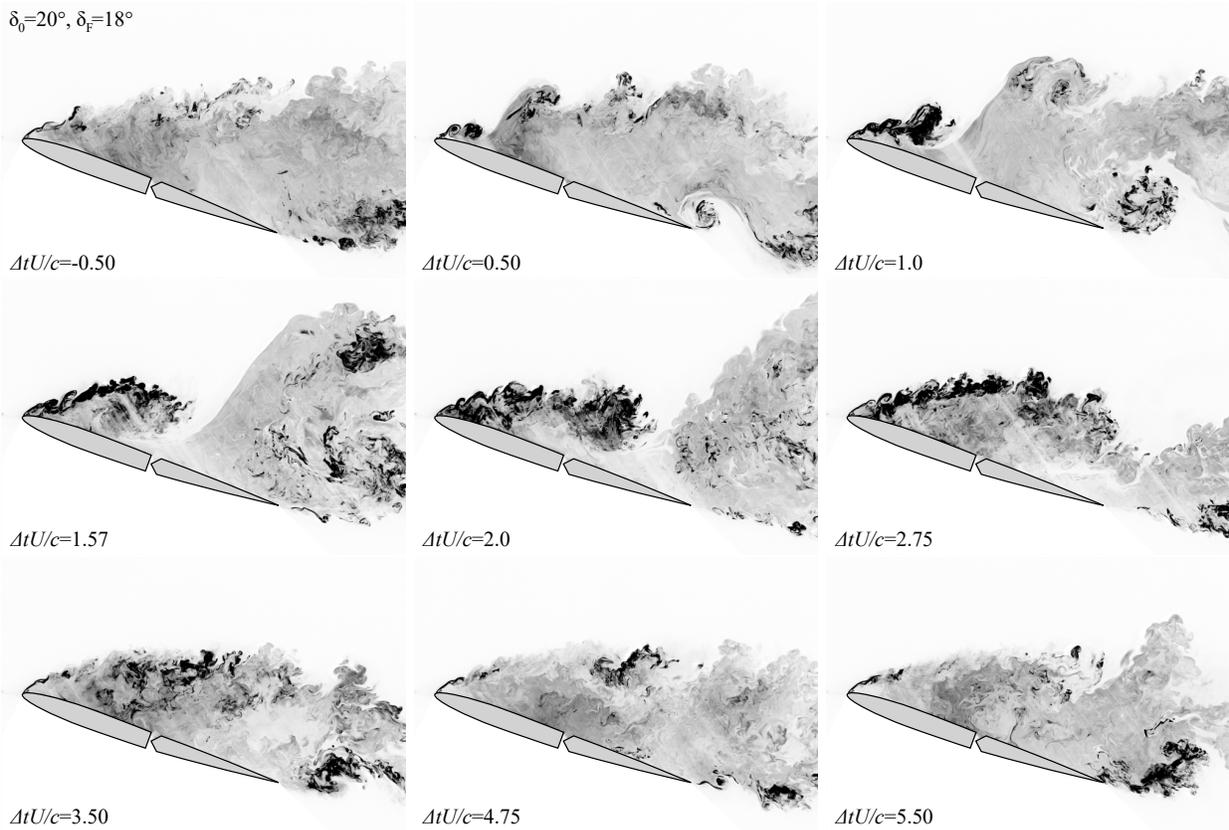$\Delta tU/c{=}3.50$ $\qquad$ $\Delta tU/c{=}4.75$ $\qquad$ $\Delta tU/c{=}5.50$

Figure 7. Flow visualization of the temporal evolution of vortical formations in response to a single rapid flap deflection ramp: $\Delta\delta = -2°$ (net decrease in positive camber) at $f = 6\text{Hz}$.

The mechanisms by which the deflection schedule of $\Delta\delta = +2°$ induces an instantaneous increment in lift remains a curious prospect. The flow field response to a net-increase-positive-camber ramp is visualized in Fig. 8. Given the shared initial state of $\delta = 20°$ there is negligible difference at $tU/c = -0.5$ between $\Delta\delta = -2°$ and $+2°$. The similarities depart as soon as $tU/c = 0.5$, shortly after performing the ramp motion. Key differences include the mitigated convection of the start-up trailing-edge vortex and a disunited roll-up of the shear layer. The new orientation of the airfoil effectively acts to shields the vortex from the freestream velocity. There remains little remnant of the stopping vortex as its circulation has been nominally neutralized in part by the freestream. As such, the dominant trailing-edge and leading-edge formations are of the same rotational direction between $\Delta\delta = -2°$ and $+2°$. However, the disparity in trailing-edge vortex size is apparent. Inspection of the leading edge region reveals a series of discrete roll-up sites about the shear layer rather than a singular structure as observed for $\Delta\delta = -2°$. This would suggest the current deflection direction is conducive to a weaker disruption of the leading-edge shear layer. Nevertheless, the resulting flow field produces an immediate incremented lift profile. The differences cited in leading-edge formations are ameliorated by $tU/c = 1.0$ where the observation of a singular distinct leading-edge vortex is apparent. And just as before this phase of the flow field is marked by the leading-edge vortex induced downwash promoting reattachment and the ejection of the separated region from atop the airfoil. Notable differences now pertain to the proximity of the trailing-edge vortex. At $tU/c = 1.63$ it becomes clear the circulatory strength of the leading-edge vortex is insufficient in establishing flow reattachment. It is also noted that the trailing-edge vortex has convected out of frame being replaced by a trailing-edge shear layer. Peak lift production at $tU/c = 2.38$ amounts to a diffused leading-edge vortex with oriented along the airfoil surface and is coincident with the passage of the initial separated plume downstream from the trailing edge. Once more, as lift descends during $tU/c = 3.10$ the leading-edge shear layer trajectory is further removed from the airfoil and the near wake constitutes a narrow band. Lastly, with the shedding of a secondary trailing-edge vortex a secondary lift peak is generated at $tU/c = 5.0$.
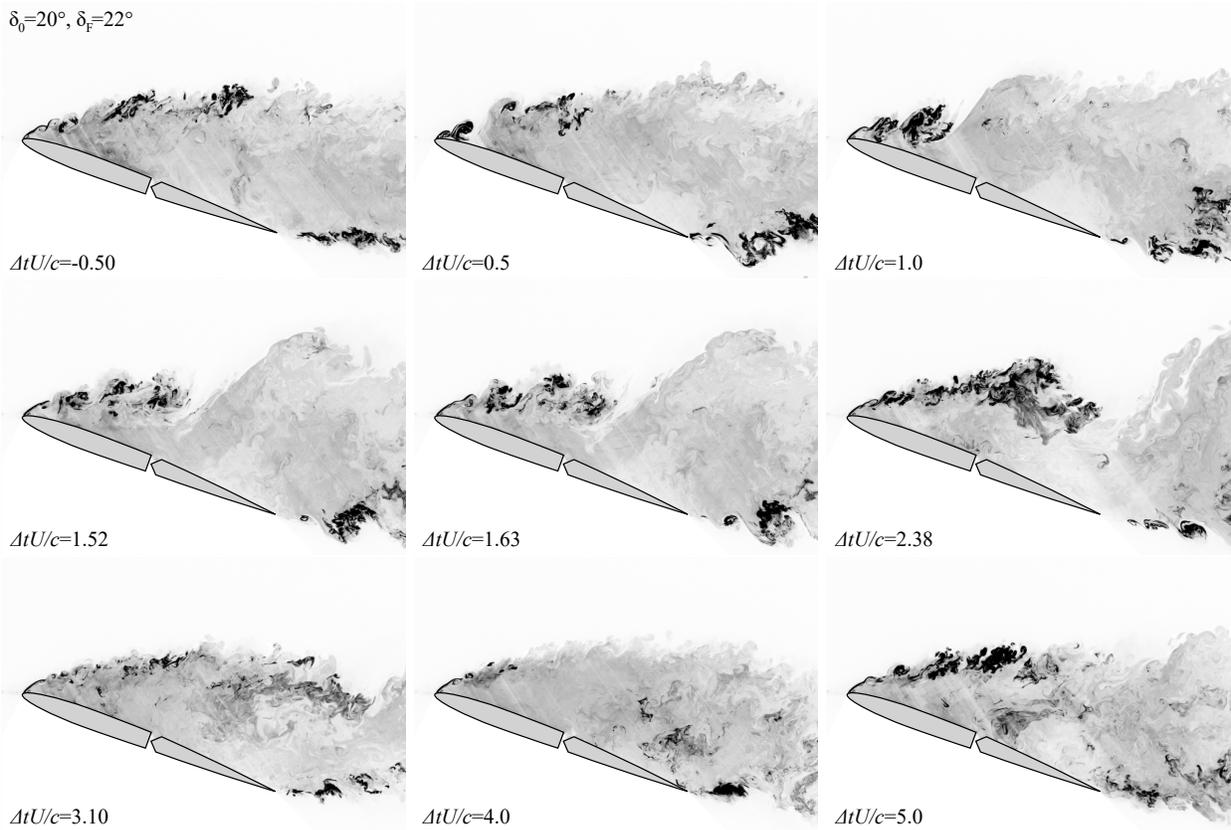
American Institute of Aeronautics and Astronautics

$\delta_0 = 20°$, $\delta_F = 22°$

$\Delta tU/c=$-0.50

$\Delta tU/c=$0.5

$\Delta tU/c=$1.0

$\Delta tU/c=$1.52

$\Delta tU/c=$1.63

$\Delta tU/c=$2.38

$\Delta tU/c=$3.10

$\Delta tU/c=$4.0

$\Delta tU/c=$5.0

Figure 8. Flow visualization of the temporal evolution of vortical formations in response to a single rapid flap deflection ramp: $\Delta\delta = +2°$ (net increase in positive camber) at $f = 6$Hz.

D.   Modal Decomposition

Independent of flap direction, the rapid-flap ramp-motion yields the formation of a coherent leading-edge vortex. Select snapshots showcasing the initial roll-up of the LEV shortly after actuation at $tU/c = 1.0$ and vortical formations coincident with peak lift production are displayed in the vorticity fields of Fig. 9. As previously surmised from qualitative dye visualization, the newly generated leading-edge vortex displaces the separation envelope from atop the airfoil. Greater proximity between the LEV and the airfoil surface, however, is observed for $\Delta\delta = -2°$ deflection. In both instances of actuation, during peak transient lift production, the LEV has appreciated to a re-circulating region occupying much of the airfoil chord as the initial separation envelope is removed in its convection downstream.
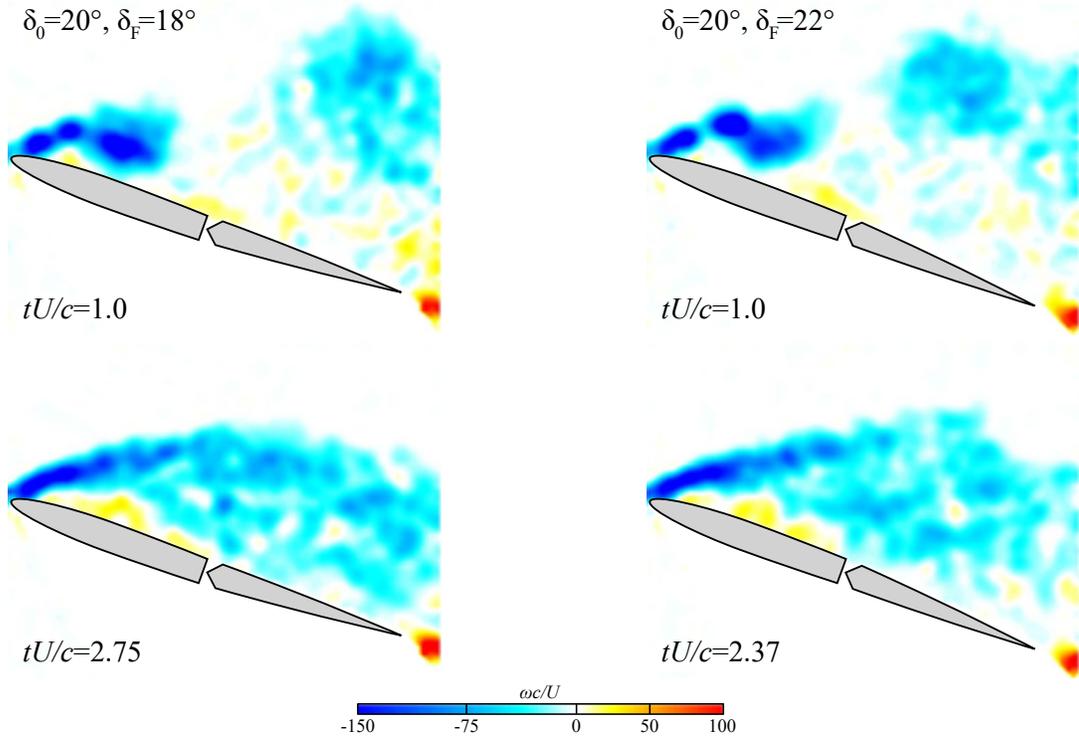
American Institute of Aeronautics and Astronautics

δ_0=20°, δ_F=18° δ_0=20°, δ_F=22°

tU/c=1.0 tU/c=1.0

tU/c=2.75 tU/c=2.37

$\omega c/U$

-150   -75   0   50   100

Figure 9. Vorticity fields for $f = 6$Hz: (*left*) $\Delta\delta = -2°$, (*right*) $\Delta\delta = +2°$.

Despite markedly similar flow field responses garnered among the two modes of actuation (albeit with potential temporal offsets) the mechanisms distinguishing the instantaneous incremented lift of $\Delta\delta = +2°$ from the classical initial 'lift reversal' shared by $\Delta\delta = -2°$ flap actuation remain elusive. To help elucidate these distinctive outputs, snapshot proper orthogonal decomposition with baseline subtraction was performed on the vorticity fields to reduce the flow features to a small number of linearly uncorrelated modes [16]. Results are presented in Fig. 10. Analysis here is limited to the 6 most energetic modes. The cumulative normalized energy is shown in Fig. 11. The most energetic modes among the two ramp cases, mode 1 and 2, are largely representative of shear layer coherence owing to the leading-edge incidence. Each respective mode appears to bear similar features between the two ramp directions. Between $\Delta\delta = -2°$ and $+2°$, however, mode 3 presents the nominal polar opposite in response to opposite kinematic schedules. Examination of the temporal coefficient of mode 3 in Fig. 12 demonstrates an increase for $\Delta\delta = -2°$ and a decrease in the coefficient for $\Delta\delta = +2°$ immediately following actuation. This is in stark contrast to the remaining modal coefficients which share a common temporal evolution. The mechanisms by which the two force responses are arrived would appear to be the promotion of leading-edge shear for $\Delta\delta = -2°$ and the retardation of leading-edge shear for the $\Delta\delta = +2°$ counterpart. The brief pivoting motion of the flap may be viewed as a momentary step in bound circulation. In deflecting toward a net increase in camber, $-2°$, it is hypothesized that the hydrodynamically coupled stationary fore element adopts a counter-clockwise circulation increment. Upon the flap completing its rapid ramp, this bound counter-clockwise circulation increment is fluxed into the flow field near the leading edge where it weakens the shear layer by neutralizing counter-rotating vorticity. The result is the severing of the shear layer from the separation envelope. Conversely, for $\Delta\delta = +2°$, their exists a flux of clockwise vorticity near the leading edge as the flap comes to a stop. Once again there is disruption of the shear layer from the separation envelope by virtue of a surge in shear layer roll-up.
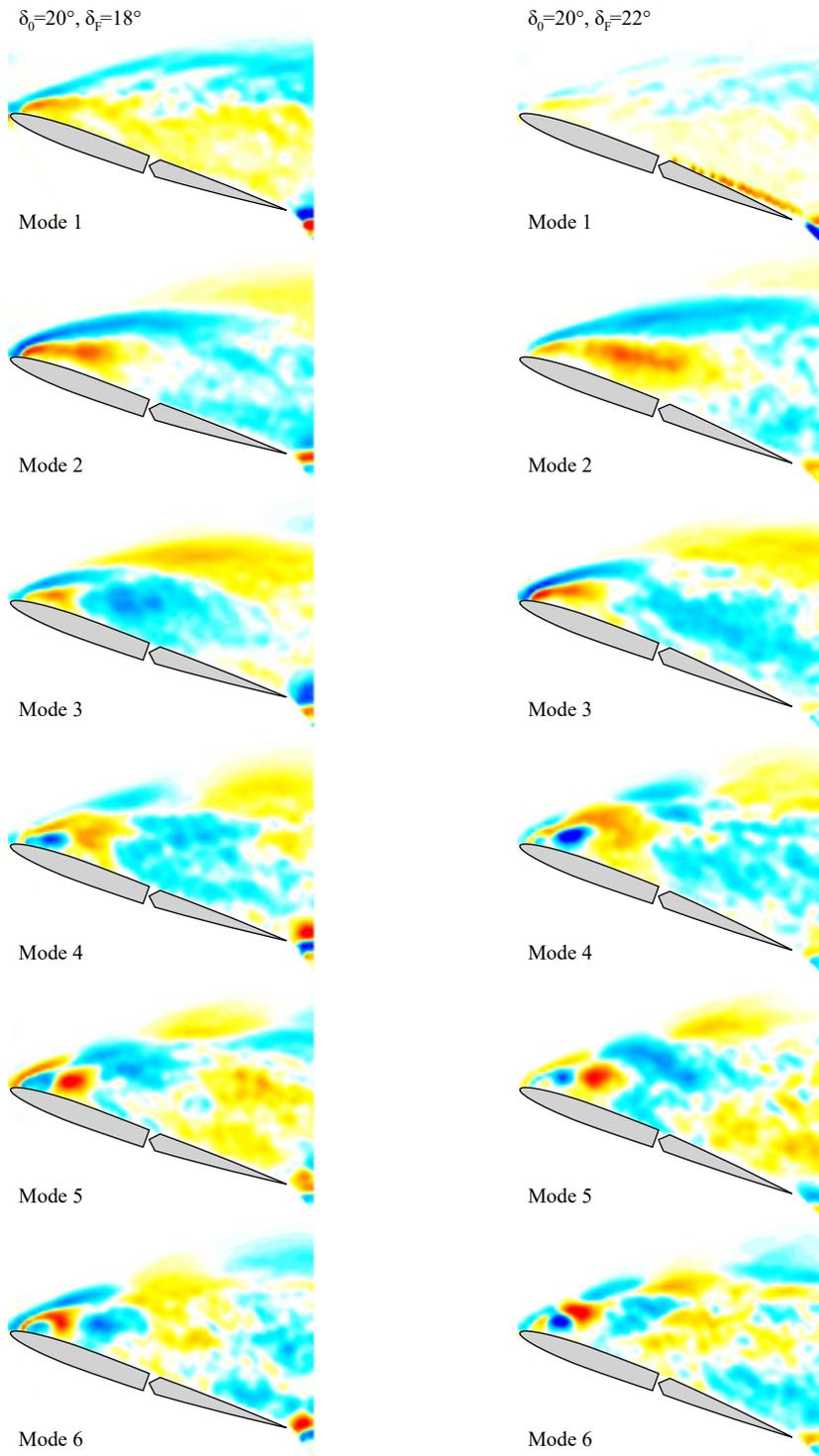
American Institute of Aeronautics and Astronautics

$\delta_0=20°, \delta_F=18°$ $\delta_0=20°, \delta_F=22°$

Mode 1

Mode 2

Mode 3

Mode 4

Mode 5

Mode 6

Figure 10. POD modes 1-6 for $f = 6$Hz: (*left*) $\Delta\delta = -2°$, (*right*) $\Delta\delta = +2°$.
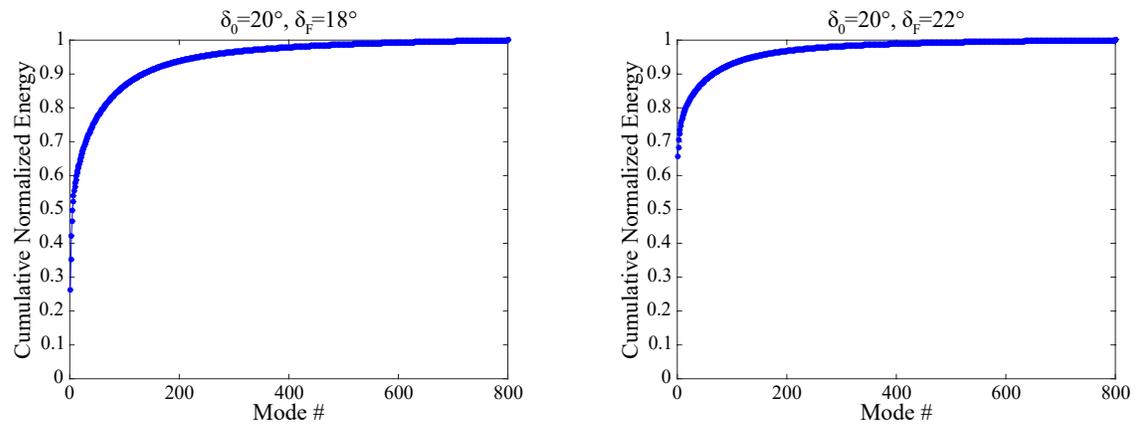
American Institute of Aeronautics and Astronautics

Figure 11. Cumulative normalized energy of POD modes for $f = 6\text{Hz}$: (*left*) $\Delta\delta = -2°$, (*right*) $\Delta\delta = +2°$.
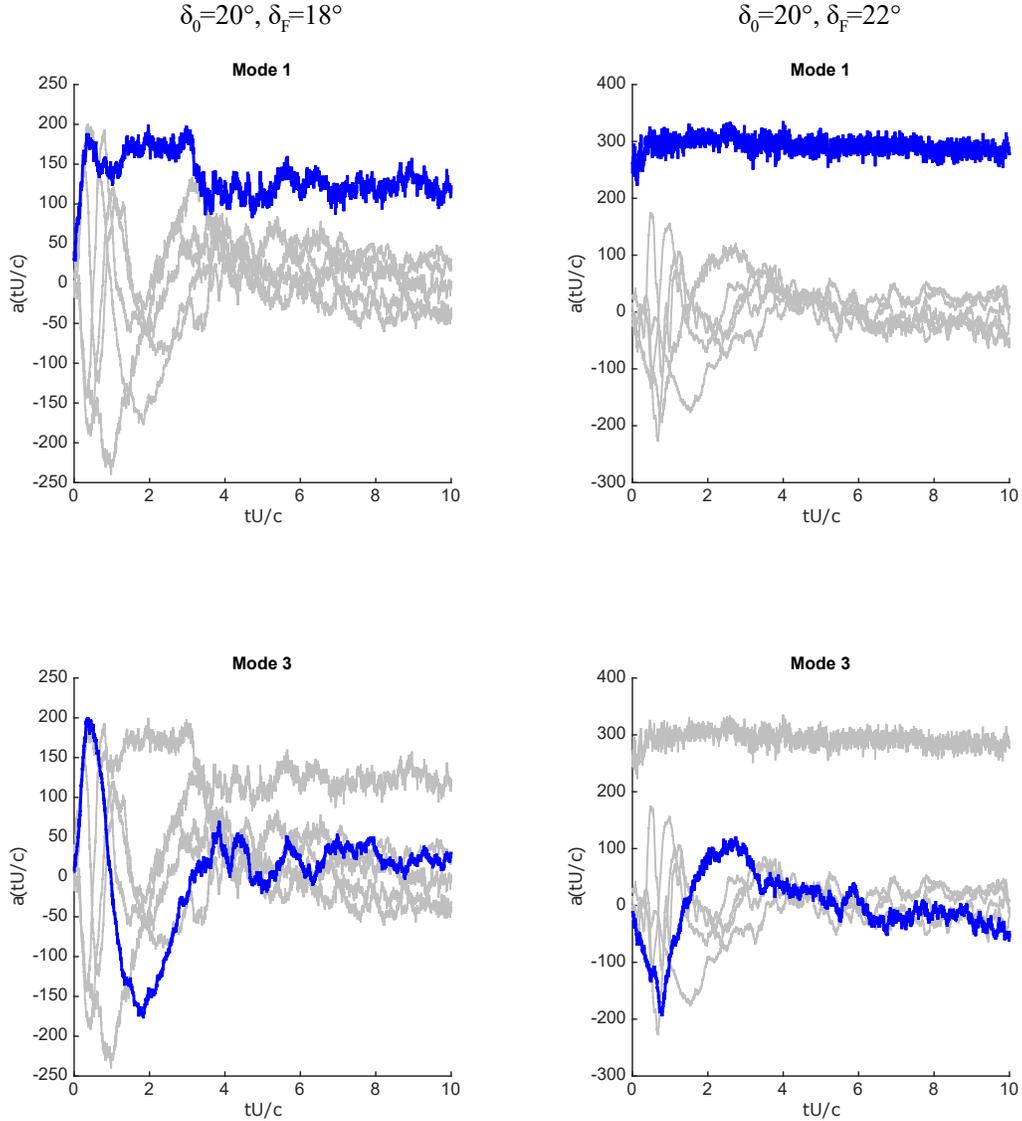
American Institute of Aeronautics and Astronautics

Figure 12. Temporal coefficient values for POD modes of Fig. 10: (*left*) $\Delta\delta = -2°$, (*right*) $\Delta\delta = +2°$.

IV. Conclusion

The transient effects of low-amplitude high-rate ramp motion of a flap on the lift and drag forces of a massively separated NACA0006 airfoil were examined. It was found that the ensuing force transients were highly dependent on the direction of flap actuation. In performing a ramp motion of $\Delta\delta = -2°$, which amounts to a net decrease in positive camber, the transient lift response bore the hallmarks of conventional control schemes: an initial anti-lift spike, followed by lift recovery, then a surge in lift to a global maximum, then a gradual recovery to resume steady state performance. In reversing the ramp direction ($\Delta\delta = +2°$), the transient force response is devoid of the deleterious anti-lift spike, but instead produces an immediate incremented lift exceeding the steady state performance. Regardless of ramp direction, it appeared that the duration of transients remained unaffected. The lift transients of negative-camber motion ($\Delta\delta = -2°$) demonstrated a greater dependency on ramp rate. Conversely, there appeared to be less dependency on ramp rate for positive-camber transients ($\Delta\delta = +2°$) up until a hypothesized threshold. Although both cases of deflection were unified in their formation of leading- and trailing-edge vortices, POD analysis revealed bifurcation of the flow field in response to flap actuation. Of the most energetic modes examined, a single

American Institute of Aeronautics and Astronautics

mode was found to have a temporal-coefficient polarity-shift pending flap direction.

Acknowledgments

References

[1] Williams, D., Kerstens, W., Pfeiffer, J., King, R., and Colonius, T., "Unsteady lift suppression with a robust closed loop controller," *Active Flow Control II*, edited by R. King, Vol. 108, Springer-Verlag, Heidelberg, Germany, 2010, pp. 19–30.

[2] Raju, R., Mittal, R., and Cattafesta, L., "Dynamics of airfoil separation control using zero-net-mass-flux forcing," *AIAA Journal*, Vol. 46, No. 12, 2008, pp. 3103–3115. doi:10.2514/1.37147.

[3] Albrecht, T., Weier, T., Gerbeth, G., Monnier, B., and Williams, D., "Separated flow response to single pulse actuation," *AIAA Journal*, Vol. 53, No. 1, 2015, pp. 190–199. doi:10.2514/1.J053026.

[4] Brzozowski, D., Woo, G., Culp, J., and Glezer, A., "Transient separation control using pulse-combustion actuation," *AIAA Journal*, Vol. 48, No. 11, 2010. doi:10.2514/1.45904.

[5] Amitay, M. and Glezer, A., "Role of actuation frequency in controlled flow reattachment over a stalled airfoil," *AIAA Journal*, Vol. 40, No. 2, 2002, pp. 209–216. doi:10.2514/2.1662.

[6] Amitay, M. and Glezer, A., "Flow transients induced on a 2D airfol by pulse-modulated actuation," *Experiments in Fluids*, Vol. 40, No. 2, 2006, pp. 329–331. doi:10.1007/s00348-005-0069-6.

[7] Margalit, S., Greenblatt, D., Seifert, A., and Wygnanski, I., "Delta wing stall and roll control using segmented Piezoelectric fluid actuators," *Journal of Aircraft*, Vol. 42, No. 3, 2005, pp. 698–709. doi:10.2514/1.6904.

[8] Natarajan, M., Freund, J., and Bodony, D., "Actuator selection and placement for localized feedback flow control," *Journal of Fluid Mechanics*, Vol. 809, 2016, pp. 775–792. doi:10.1017/jfm.2016.700.

[9] Chomaz, J., "Global instabilities in spatially developing in flows: non-normality and nonlinearlity," *Annual Review of Fluid Mechanics*, Vol. 37, 2005, pp. 357–391. doi:10.1146/annurev.fluid.37.061903.175810.

[10] Huang, L., Huang, P., and LeBeau, R., "Numerical study of blowing and suction control mechanism on NACA0012 airfoil," *Journal of Aircraft*, Vol. 41, No. 5, 2004, pp. 1005–1013. doi:10.2514/1.2255.

[11] Granlund, K., Monnier, B., Ol, M., and Williams, D., "Airfoil longitudinal gust response in separated vs attached flows," *Physics of Fluids*, Vol. 26, No. 2, 2014, pp. 027103. doi:10.1063/1.4864338.

[12] Ol, M., Eldredge, J., and Wang, C., "High-amplitude pitch of a flat plate: an abstraction of perching and flapping," *International Journal of MAVs*, Vol. 1, No. 3, 2009, pp. 203–216. doi:10.1260/175682909789996186.

[13] Granlund, K., Ol, M., and Bernal, L., "Unsteady pitching flat plates," *Journal of Fluid Mechanics*, Vol. 733, 2013, pp. R5. doi:10.1017/jfm.2013.444.

[14] Medina, A., Ol, M., Williams, D., An, X., and Hemati, M., "Modeling of conventional flaps at High Deflection-Rate," *55th AIAA Aerospace Sciences Meeting, AIAA SciTech Forum*, (AIAA 2017-1230), Grapevine, Texas, 2017. doi:10.2514/6.2017-1230.

[15] Medina, A., Ol, M., Mancini, P., and Jones, A., "Revisiting conventional flaps at high deflection rate," *AIAA Journal*, Vol. 55, No. 8, 2017, pp. 2676–2685. doi:10.2514/1.J055754.

[16] Holmes, P., Lumley, J., and Berkooz, G., *Turbulence, coherent structures, dynamical systems and symmetry*, Cambridge Univ. Press, 2nd ed., 2012.

American Institute of Aeronautics and Astronautics